Journal of Nuclear Materials 393 (2009) 120–125

Contents lists available at ScienceDirect

Journal of Nuclear Materials

journal homepage: www.elsevier.com/locate/jnucmat

XPS analysis of $U_xCe_{1-x}O_{2\pm\delta}$ and determination of oxygen to metal ratio

Santanu Bera [a,*], V.K. Mittal [a], R. Venkata Krishnan [b], T. Saravanan [a], S. Velmurugan [a], K. Nagarajan [b], S.V. Narasimhan [a]

[a] Water and Steam Chemistry Division, BARC Facilities, Kalpakkam 603 102, Tamil Nadu, India
[b] Fuel Chemistry Division, IGCAR, Kalpakkam 603 102, Tamil Nadu, India

ARTICLE INFO

Article history:
Received 18 December 2007
Accepted 26 May 2009

ABSTRACT

The chemical states of U and Ce in the solid solutions of UO_2 and CeO_2 are studied using the X-ray photoelectron spectroscopy. A detailed analyses on U 4f and Ce 3d photoelectron peaks revealed the presence of Ce^{3+} and U^{5+}/U^{6+} states in the mixed oxides. The oxygen to metal ratios in different compositions of mixed oxides were estimated from the quantity of different chemical states of U and Ce present in mixed oxides.

1. Introduction

Cerium is one of the major fission products of uranium containing nuclear fuels. Therefore knowledge of chemical phases and oxygen stoichiometry in $U_xCe_{1-x}O_{2\pm\delta}$ are of basic importance to understand the behavior of uranium dioxide fuel under irradiation conditions [1–3]. Uranium and cerium dioxide are known to form solid solution covering a wide compositional range of Ce (2–90 at.%) content due to their structural similarity [2–5]. Various properties have been studied in past on varying composition of $U_xCe_{1-x}O_{2\pm\delta}$ mixed oxides [6–8]. Most of the data available in the literature are on measurement of electrical conductivity [6], thermal expansion [1], oxygen potential [7], lattice parameter [8] and heat capacity [4]. Oxidation behavior of $U_xCe_{1-x}O_{2\pm\delta}$ systems have been studied using the X-ray photoelectron spectroscopy (XPS) technique [9]. The presence of U^{5+} and Ce^{4+} was detected by XPS technique in oxidized U–Ce oxides containing different amount of Ce [9]. However, a detailed XPS analysis on chemical states of U and Ce in U–Ce mixed oxides is still lacking. Detailed chemical analysis of U and Ce in $U_xCe_{1-x}O_{2\pm\delta}$ may not only be of academic interest, but it is expected to offer guidelines for explaining the oxidation and storage behavior of the mixed oxides.

In the case of pure CeO_2, existence of Ce^{3+} is always expected due to presence of oxygen vacancy, especially at the surface of the samples. Similarly, UO_2 is also known to be unstable in air and gets oxidized to higher oxidation states, thus creating UO_{2+x} type oxide [10]. Hence, it is interesting to investigate chemical states of U and Ce in their solid solutions of mixed oxides which has not been studied. In this paper, a detail analysis on chemical states of U and Ce in $U_xCe_{1-x}O_{2\pm\delta}$, obtained from XPS, is presented. U $4f_{7/2}$ and Ce 3d photoelectron spectral line shapes were analyzed to estimate the relative atomic concentrations of different chemical states of U and Ce in the mixed oxides. In addition, these results have helped us to quantify the reacted oxygen content in the oxides. As the depth of information in XPS is limited to few nanometers from the surface of the sample, the oxygen to metal (O:M) ratio obtained from XPS is expected to be applicable only to few atomic layers from the surface.

2. Experimental details

Mixed oxide samples of $U_xCe_{1-x}O_{2\pm\delta}$ ($x = 0.06$, 0.12, 0.20, 0.30 and 0.80) are prepared by taking stoichiometric quantities of UO_2 and CeO_2. Preparations of the mixed oxides, X-ray diffraction studies and bulk analysis of these samples have been described elsewhere [4]. XRD analyses of the samples reveal single phase formation of the oxides and the lattice parameter of the cubic phase are found to follow the Vegard's law [4]. Fine powders of the mixed oxides prepared through combustion synthesis and subsequent calcinations were compacted into pellets of 5 mm diameter weighing approximately 200 mg. The pellets were further heated at 1073 K for 4 h under a flowing stream of Ar + 8% H_2 gas equilibrated with water at 298 K to ensure that the O:M ratio of the mixed oxide is maintained at 2.0 [4]. The ratio has also been verified using a solid electrolyte (calcia stabilized zirconia based) cell [11]. Prepared samples were stored in an inert atmosphere glove box and the exposure of the sample to the atmosphere were only during the transport, handling and during XPS measurement. The approximate exposure time of the pellets will be around 4 days. However, the pellets of the mixed oxides were cleaved ex-situ and the cross-sectional new surface was loaded immediately in the analysis chamber of the XPS instrument to minimize the exposure time of the newly created surface.

XPS characterization was done using VG ESCALAB MKII system. The base vacuum of the chamber was 10^{-10} mbar and Al Kα was

* Corresponding author. Tel.: +91 44 2748 0203; fax: +91 44 2748 0097.
E-mail address: bera@igcar.gov.in (S. Bera).

0022-3115/$ - see front matter © 2009 Elsevier B.V. All rights reserved.
doi:10.1016/j.jnucmat.2009.05.015

used as the exciting source for photoelectron emission. Ceria is known to undergo reduction due to X-ray beam exposure [12,13]. It was observed that a measurable reduction of Ce^{4+} to Ce^{3+} in CeO_2 occurred on exposure to Al Kα in UHV for more than 45 min [13]. In the present case, U–Ce oxides samples were tested for X-ray beam effects using a 300 W Al Kα X-ray beam. In Fig. 1, the XPS spectra for Ce 3d at different exposure time are shown. It was observed that measurable changes were seen only after 1 h of exposure as indicated by an arrow in Fig. 1. So, the experiments were performed within 15 min duration to avoid beam induced reduction of Ce^{4+}.

The spectra were acquired by a hemispherical analyzer with 150 mm mean radius at 20 eV pass energy and the surface compositions was quantified by measuring the areas under Ce3d and U $4f_{7/2}$ photoelectron peaks and standard sensitivity values available in the hand book of XPS for data analysis [14]. The deconvolutions of the spectra were carried out using standard software 'Eclipse V2.1' integrated with the data acquisition software. The component spectra were fitted with Gaussian–Lorentzian peak functions on a Shirley background. Uranium $4f_{7/2}$ peaks were fitted using standard peak width and peak positions for U^{4+} and U^{6+} peaks [15].

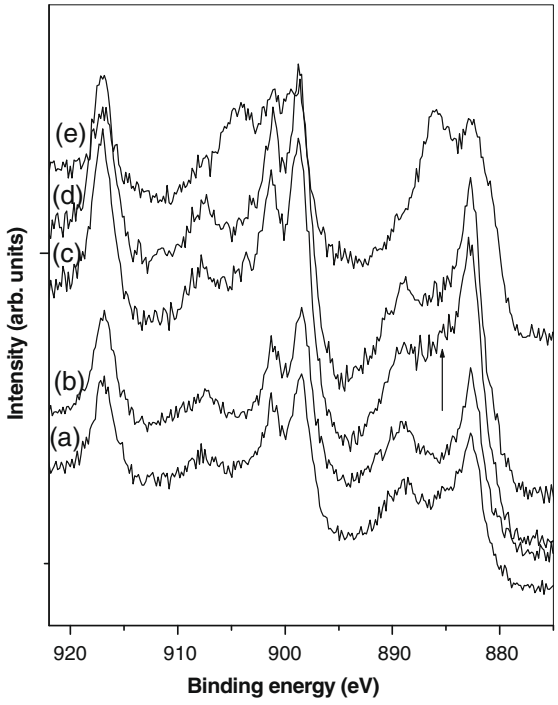

Fig. 1. Ce 3d XPS spectra acquired from $Ce_{0.80}U_{0.20}O_{2\pm\delta}$ with different X-ray beam exposure; (a) as loaded sample, (b) 15 min irradiation, (c) 1 h irradiation, (d) 2 h irradiation and (e) after Ar ion beam sputtering for 5 min.

3. Results and discussion

In XPS, the escape depth depends upon the mean free path of the photoelectrons emerging from the materials. The mean free path for U 4f and Ce 3d photoelectrons was calculated to be around 1.8–1.9 nm and the total escape depth was found to be around 6.0 nm from the surface of the sample [16,17]. So, the information obtained from the technique is specifically limited to the surface of the crystallites. In situ sputtering using Ar^+ ion beam is a widely used technique to remove multiple layers to acquire bulk information of the materials. But we observed that these oxides undergo tremendous reduction even after a short exposure (5 min) of 3 keV Ar^+ ion beam with ~2 μA sample current (Fig. 1(e)). So, to avoid the ion beam damage on the samples, sputtering was not used to obtain O:M ratio information at the bulk.

3.1. U 4f photoelectron peak analysis

The binding energy of U $4f_{7/2}$ photoelectron is very sensitive towards oxidation state and shows positive chemical shift with increasing oxidation states. In Table 1, binding energy values of U and its various oxides (U^{4+} and U^{6+}) are given along with the full width at half maximum (FWHM) values [15].

Measured photoelectron peak width (FWHM) is the convolution of energy-width of the X-ray source, analyzer resolution and the natural width of the core levels. The first two widths are fixed for an instrument and hence the FWHM of U $4f_{7/2}$ is related to the width of the excited state which is directly dependent on the chemical environment or bonding. Thus, the photoelectron peak width is an important parameter for chemical state analysis. In case, photoelectron peaks from two different chemical states of the same element are lying very close, they may overlap to give single peak with larger FWHM. Composite peaks are resolved by fitting the Gaussian–Lorentzian line-shape functions using the peak position and FWHM values for the respective oxidation states taken from similar standard compounds.

The peak binding energy and the peak widths for U $4f_{7/2}$ in different $U_xCe_{1-x}O_{2\pm\delta}$ oxides are presented in Table 1. Measured peak widths are higher than that either U^{4+} or U^{6+} chemical states. Hence, the peaks are deconvoluted into two peaks corresponding to various chemical states of U as shown in Fig. 2. Table 1 shows the deconvolution parameters of different chemical states of U in different $U_xCe_{1-x}O_{2\pm\delta}$ compounds. In case of $U_{0.80}Ce_{0.20}O_{2\pm\delta}$ and $U_{0.30}Ce_{0.70}O_{2\pm\delta}$ samples, the presence of U^{5+} is seen after deconvoluting the spectra.

Satellite of U 4f photoelectron spectrum is found to be very useful in identifying the chemical states of U [18]. In Fig. 3, U 4f spectra obtained from two different samples like $U_{0.12}Ce_{0.88}O_{2\pm\delta}$ and $U_{0.80}Ce_{0.20}O_{2\pm\delta}$ are shown. In case of $U_{0.12}Ce_{0.88}O_{2\pm\delta}$, a distinct satellite at around 6.5 eV corresponding to U^{4+} has been seen. In case of $U_{0.80}Ce_{0.20}O_{2\pm\delta}$ the satellite position at around 8.2 eV confirms the presence of the U^{5+} [15,18].

Table 1
Binding energy of U $4f_{7/2}$ photoelectron peaks recorded from different U standards and U–Ce mixed oxides. The peak positions of the deconvoluted peaks are presented.

Sample	U $4f_{7/2}$ (FWHM)	Deconvoluted U $4f_{7/2}$ (FWHM) (eV)		
	(eV)	U^{4+}	U^{5+}	U^{6+}
U^0	377.2			
U^{4+}	379.9 (2.2)			
U^{6+}	381.1 (2.5)			
$U_{0.06}Ce_{0.94}O_{2\pm\delta}$	379.8 (2.6)	379.7 (2.2)		381.1 (2.5)
$U_{0.12}Ce_{0.88}O_{2\pm\delta}$	380.2 (2.7)	379.9 (2.2)		381.1 (2.4)
$U_{0.20}Ce_{0.80}O_{2\pm\delta}$	380.2 (2.9)	379.7 (2.2)		381.0 (2.4)
$U_{0.30}Ce_{0.70}O_{2\pm\delta}$	380.7 (2.5)	380.1 (2.2)	380.7 (2.4)	
$U_{0.80}Ce_{0.20}O_{2\pm\delta}$	380.6 (2.5)	380.2 (2.2)	380.7 (2.4)	

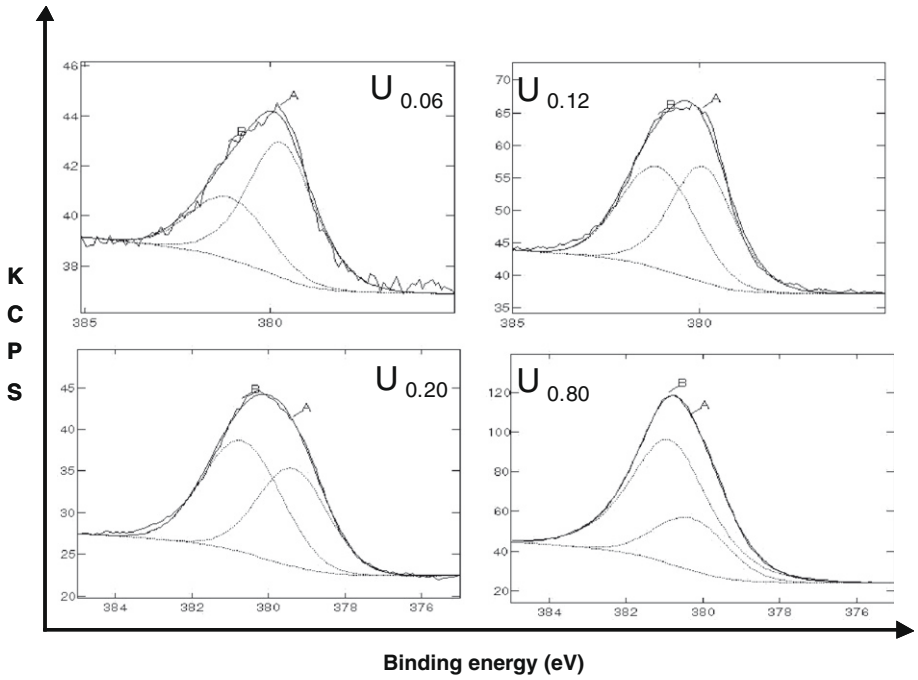

Fig. 2. Deconvolution of U 4f $_{7/2}$ recorded from $U_xCe_{1-x}O_{2\pm\delta}$ mixed oxides for x = 0.06, 0.12, 0.20 and 0.80.

3.2. Ce 3d photoelectron peak analysis

Usually, Ce 3d spectrum from CeO_2 contains a spin orbit doublet of $3d_{5/2}$ and $3d_{3/2}$. In addition to these two peaks, it exhibits a three-peak structure in each of $3d_{3/2}$ and $3d_{5/2}$ components (a total of six peaks) due to different final states in the O 2p and Ce 4f valance orbital [19]. In the present case of mixed Ce^{3+} and Ce^{4+} systems, Ce 3d spectra present ten peaks with six distinct contributions from Ce^{4+} and four distinct components from Ce^{3+}. The Ce 3d spectra obtained from $U_xCe_{1-x}O_{2\pm\delta}$ are observed to show spectral features similar to CeO_2. The main Ce 3d peaks and its satellites obtained from $U_{0.06}Ce_{0.94}O_{2\pm\delta}$ are presented in Table 2. In case of Ce^{3+}, u_0 and u_1 (Table 2) are the main component and shake-down peaks respectively from $3d_{5/2}$ and u'_0 and u'_1 correspond to that for the $3d_{3/2}$ contribution. For Ce^{4+}, v_2 and v'_2 peaks are the principal $3d_{5/2}$ and $3d_{3/2}$ contributions. The peaks v_0, v_1 are associated with $3d_{5/2}$ and v'_0 and v'_1 are the satellites for $3d_{3/2}$. The initial and final states contributing to the Ce 3d spectra [19] are given in Table 2. Ce 3d peak parameters of other U–Ce oxides obtained through deconvolutions have been used to quantify Ce^{3+} and Ce^{4+} in the mixed oxide samples. The detailed deconvolutions of Ce 3d peaks are shown in Fig. 4.

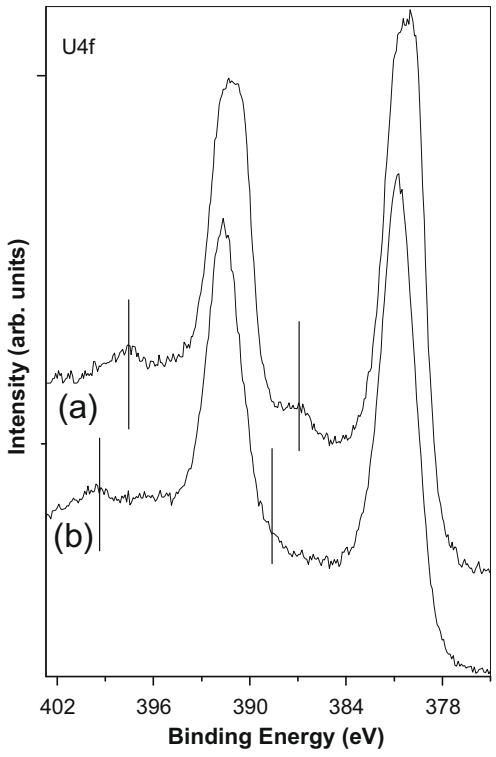

Fig. 3. U 4f photoelectron spectra obtained from (a) $U_{0.12}Ce_{0.88}O_{2\pm\delta}$ and (b) $U_{0.80}Ce_{0.20}O_{2\pm\delta}$. A distinct satellite (marked by vertical line) observed at 8.2 eV above the principal 4f peak in $U_{0.80}Ce_{0.20}O_{2\pm\delta}$ indicates the presence of U^{5+}.

Presence of all these ten peaks in Ce 3d spectra makes the fitting very complicated and renders it difficult to quantify different chemical states present in the samples. In general, two methods are followed to find the concentration of Ce^{3+} and Ce^{4+} in a convoluted Ce 3d peak, such as, factor analysis and deconvolution of Ce 3d peak through suitable Gaussian– Lorentzian peak fitting. These two methods produce equivalent results [20,21]. Ce 3d peaks, obtained from different $U_xCe_{1-x}O_{2\pm\delta}$ samples, have been deconvoluted by curve fitting method. Two additional peaks (marked as s1 and s2) known to be shake up satellites of main Ce^{3+} component [20] are used for the fitting. The peak widths and peak positions for the different peaks are kept same while fitting the Ce 3d peak recorded from other $U_xCe_{1-x}O_{2\pm\delta}$. An efficient method was suggested by Romeo et al. [22] where all the peaks were used to determine Ce^{3+} content. The concentration of Ce^{3+} is calculated from the following equation [22],

$$Ce^{3+} = \frac{u_1 + u'_1 + u_0 + u'_0 + s_1 + s_2}{\text{total area of Ce 3d}} = \text{integral area of } Ce^{3+}/\text{total area of } (Ce^{3+} + Ce^{4+}).$$

In Table 3, calculated concentrations of Ce^{3+} in different mixed oxides are shown.

Table 2
Origin of different satellites of Ce 3d photoelectron peaks from $U_{0.06}Ce_{0.94}O_{2\pm\delta}$ (v represents the valence band; S represents satellite).

Ce ion	Initial state	Final state	Peaks Ce 3d (eV)	FWHM (eV)	Origin	Notation
Ce^{3+}	$3d^{10}4f^{1}$	$3d^{9}4f^{2}v^{n-1}$	881.2	2.7	S-$3d_{5/2}$	u_1
			900.0	2.5	S-$3d_{3/2}$	u'_1
		$3d^{9}4f^{1}v^{n}$	885.0	3.2	Main-$3d_{5/2}$	u_0
			903.7	3.6	Main-$3d_{3/2}$	u'_0
			895.3	4.0	Added-satellite	s_1
			913.0	4.0	Added-satellite	s_2
Ce^{4+}	$3d^{10}4f^{0}$	$3d^{9}4f^{2}v^{n-2}$	882.8	2.2	S1-$3d_{5/2}$	v_0
			901.3	2.1	S1-$3d_{3/2}$	v'_0
		$3d^{9}4f^{1}v^{n-1}$	888.9	5.8	S2-$3d_{5/2}$	v_1
			907.6	4.6	S2-$3d_{3/2}$	v'_1
		$3d^{9}4f^{0}v^{n}$	898.5	2.4	Main-$3d_{5/2}$	v_2
			917.1	2.7	Main-$3d_{3/2}$	v'_2

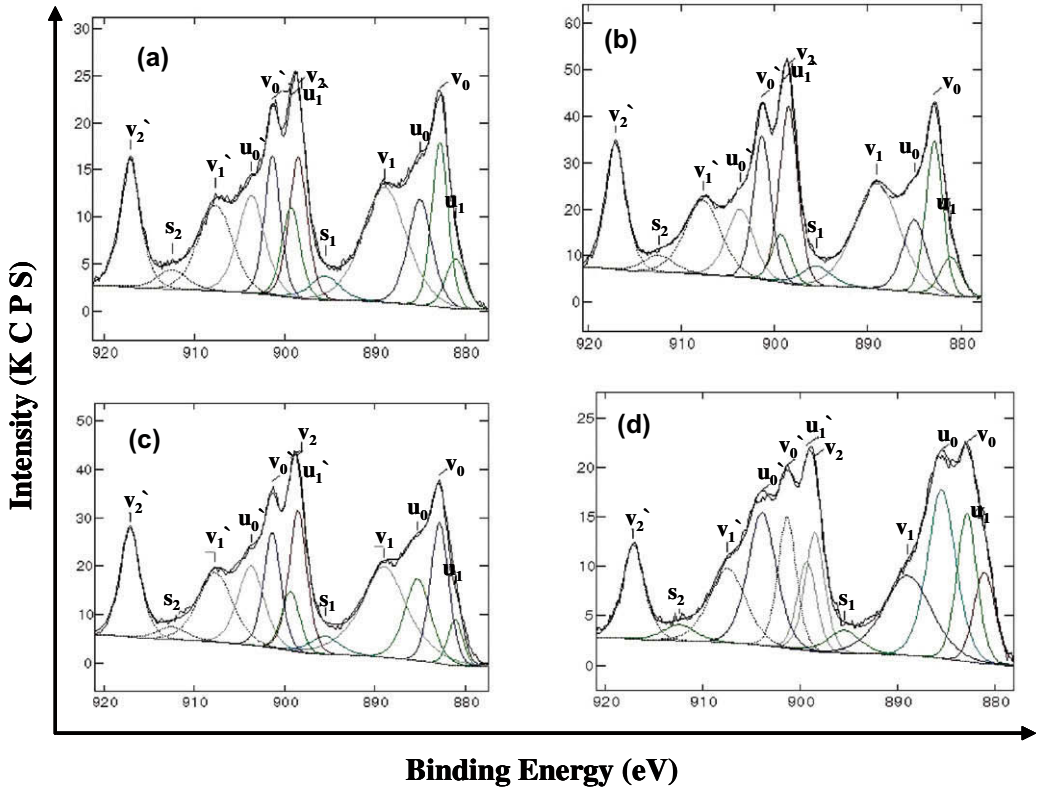

Fig. 4. Deconvolution of Ce 3d photoelectron spectra obtained from various oxide samples (a) $U_{0.06}Ce_{0.94}O_{2\pm\delta}$, (b) $U_{0.20}Ce_{0.80}O_{2\pm\delta}$, (c) $U_{0.30}Ce_{0.70}O_{2\pm\delta}$ and (d) $U_{0.80}Ce_{0.20}O_{2\pm\delta}$.

3.3. Compositional analysis

The peak area under U $4f_{7/2}$ and Ce 3d photoelectron peaks were measured to calculate the relative atomic concentration of the elements taking into account of their respective standard sensitivity values [14]. In Table 3, surface composition of different $U_xCe_{1-x}O_{2\pm\delta}$ (for x ranging from 0.06 to 0.80) is presented. It is observed here that $U_xCe_{1-x}O_{2\pm\delta}$ samples have multiple oxidation states for both U and Ce. Uranium in $U_xCe_{1-x}O_{2\pm\delta}$ oxides with U concentrations ranging from 0.06 to 0.20 are present in U^{4+} and U^{6+} states. With increasing concentration of U (x = 0.30 and 0.80) it is present dominantly in U^{5+} states. Ce is found to be present in both Ce^{3+} and Ce^{4+} states. Thus, the oxides stabilize as a mixture of different states of U and Ce to give the total charge neutrality in the material. In Table 3, the atomic % of different chemical states of U and Ce are given. Further it is observed here that the amount of U^{4+} gradually reduced as the U content in the sample increased (Fig. 5).

Table 3
Atomic concentration (at.%) of U and Ce obtained from the XPS analysis.

Sample	U at.%	Ce at.%	Ce^{3+}% of total Ce	U^{x+} at.% of total U		
				U^{4+}	U^{5+}	U^{6+}
$U_{0.06}Ce_{0.94}O_{2\pm\delta}$	5	95	33	66		34
$U_{0.12}Ce_{0.88}O_{2\pm\delta}$	9	91	26	50		50
$U_{0.20}Ce_{0.80}O_{2\pm\delta}$	15	85	26	44		56
$U_{0.30}Ce_{0.70}O_{2\pm\delta}$	35	65	30	22	78	
$U_{0.80}Ce_{0.20}O_{2\pm\delta}$	88	12	44	27	73	

Oxygen to metal ratio (O:M) at the surface can be estimated easily from the peak area under O1s and the peak area of U and Ce photoelectrons. Since the surface is usually contaminated with adsorbed oxygen, calculation of oxygen content from the spectra may lead to a wrong estimation of oxygen involved in the reaction. The amount of reacted oxygen on the surface depends on the chemical states of the metals below the oxygen layer [23,24]. Thus from the knowledge of chemical states of U and Ce, amount of

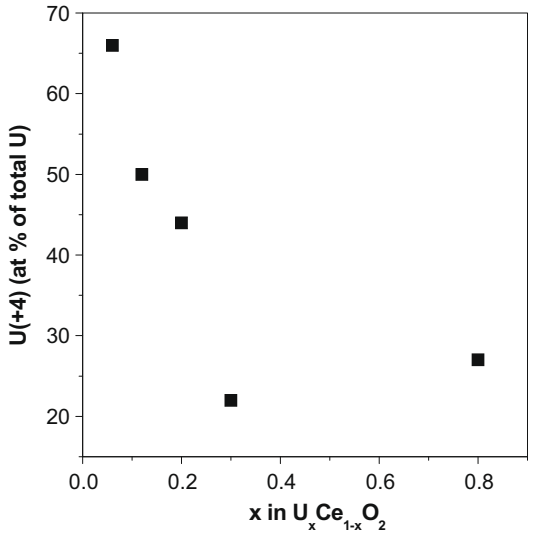

Fig. 5. Variation of U^{4+} with total U content in different U–Ce mixed oxides (from Table 3).

Table 4
Oxygen stoichiometry in $U_xCe_{1-x}O_{2\pm\delta}$ obtained from XPS analysis.

Sample	From U and Ce atomic % derived from XPS
$U_{0.06}Ce_{0.94}O_{2\pm\delta}$	$U^{4+}_{0.03}U^{6+}_{0.02}Ce^{3+}_{0.31}Ce^{4+}_{0.64}O_{1.86}$
$U_{0.12}Ce_{0.88}O_{2\pm\delta}$	$U^{4+}_{0.04}U^{6+}_{0.05}Ce^{3+}_{0.24}Ce^{4+}_{0.67}O_{1.92}$
$U_{0.20}Ce_{0.80}O_{2\pm\delta}$	$U^{4+}_{0.07}U^{6+}_{0.08}Ce^{3+}_{0.22}Ce^{4+}_{0.63}O_{1.97}$
$U_{0.30}Ce_{0.70}O_{2\pm\delta}$	$U^{4+}_{0.08}U^{5+}_{0.27}Ce^{3+}_{0.20}Ce^{4+}_{0.45}O_{2.04}$
$U_{0.80}Ce_{0.20}O_{2\pm\delta}$	$U^{4+}_{0.24}U^{5+}_{0.64}Ce^{3+}_{0.05}Ce^{4+}_{0.07}O_{2.29}$

reacted oxygen have been calculated in the mixed oxides (Table 4). This amount of oxygen seems to be necessary to obtain an equilibrium chemical structure at the surface or grain boundary in these oxides through the oxidation of U^{4+} and reduction of Ce^{4+} ions.

Assuming the charge neutrality in the oxides, different amount of oxygen obtained from the chemical state analysis is shown in Table 4. In Fig. 6, variation of calculated O:M ratio is shown as a function of uranium content. It is observed that the O:M ratio increased with the increase in U content in the material. This result agrees with previous results obtained from titrimetric method on oxidized U_xCe_{1-x} oxides [2,9]. It can be seen that the total oxygen content in the material is controlled by the dominant metal in the oxide. It appears from the XPS analysis that it could be difficult to maintain O:M ratio 2 on the oxide surface even after the heat treatment of the sample in Ar + 8% H_2 atmosphere. In Ce dominating oxides, stable oxygen vacancies are present as natural defects at the surface and grain boundary regions or created during the hydrogen treatment of the sample that reduces Ce^{4+} to Ce^{3+} in the mixed oxides. In contrary, U^{4+} has a tendency to get higher oxidation states and it may try to accommodate more oxygen at the defect sites of the surface. As a result, there will be a distribution of Ce^{3+} and U^{5+}/U^{6+} along with usual lattice of U^{4+} and Ce^{4+}. In case of higher content of Ce, the oxides show a domination of Ce^{3+} compare to U^{6+} that result lower values of O:M ratio than the expected 2.0 (Fig. 6). Similarly, when U is the major metal in the oxide, the oxygen content is controlled by U which has a tendency to accommodate more oxygen in the lattice. This would show higher oxidation states resulting in the higher oxygen in the material (Fig. 6). It appears that though the oxide crystallites show the presence of cubic phases (XRD), the presence of different states at the surface lead to the deviations of O:M ratio from 2.0 at the surface.

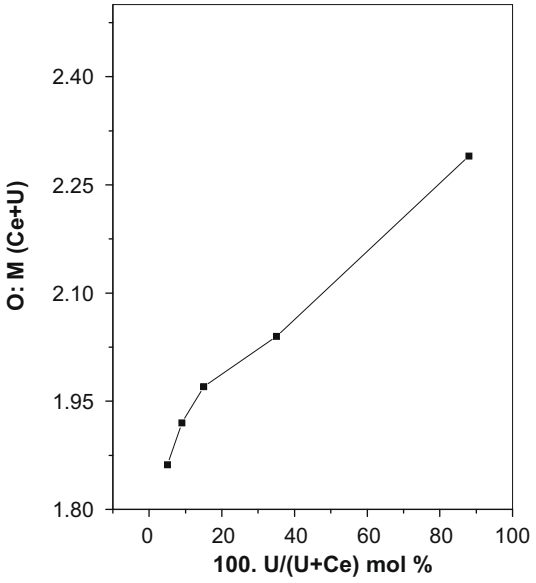

Fig. 6. Variation of oxygen to metal (O:M) ratio with respect to U content in mixed oxides obtained from XPS analysis (from Table 4).

4. Conclusions

XPS analysis is carried out on the $U_xCe_{1-x}O_{2\pm\delta}$ mixed oxide samples to find the chemical states of U and Ce. U $4f_{7/2}$ and Ce 3d photoelectron peaks are analyzed and the presence of Ce^{3+} and $U^{5+/6+}$ along with U^{4+} and Ce^{4+} states have been detected in the mixed oxide samples. The amount of reacted oxygen at the surface is estimated from the amount of different chemicals states of U and Ce in the oxides assuming the charge neutrality. Oxygen to metal ratio at surface is found to deviate from the expected value of 2.0 at the bulk of the materials and is governed by the major element (U/Ce) in the oxides. In case of U major oxides, O:M ratio is higher than 2.0 and in case of Ce major oxides the ratio is lower than 2.0. As the materials were found to be single phased in XRD, the oxygen metal ratio is mainly contributed by the lattice vacancies and defects at the surfaces.

Acknowledgements

The authors are thankful to Dr. K. Suresh Kumar of KARP, BARCF and Mr. P. Gangopadhaya, IGCAR for carefully going through the manuscript.

References

[1] Kazuhiro Yamada, Shinsuke Yamanaka, Masahiro Katsura, J. Alloys Compd. 275–277 (1998) 725.
[2] H.P. Nawada, P. Sriramamurti, K.V. Govindan Kutty, S. Rajagopalan, R.B. Yadav, P.R. Vasudeva Rao, C.K. Mathews, J. Nucl. Mater. 139 (1986) 19.
[3] Philippe Martin, Michel Ripert, Thierry Petit, Tobias Reich, Christoph Hennig, Francesco D'Acapito, Jean Louis Hazemann, Olivier Proux, J. Nucl. Mater. 312 (2003) 103.
[4] R.V. Krishnan, K. Nagarajan, Thermochim. Acta 440 (2006) 141.
[5] T.L. Markin, R.S. Street, J. Inorg. Nucl. Chem. 32 (1970) 59.
[6] S.H. Kang, J.D. Yi, H. Yoo, S.H. Kim, Y.W. Lee, J. Phys. Chem. Solids 63 (2002) 773.
[7] R. Ducroux, J. Baptiste, J. Nucl. Mater. 97 (1981) 333.
[8] D.I.R. Norris, P. Kay, J. Nucl. Mater. 116 (1983) 184.
[9] K. Suresh Kumar, H.P. Nawada, N.P. Bhat, J. Nucl. Mater. 324 (2004) 177.
[10] P.A. Tempest, P.M. Tucker, J.W. Tyler, J. Nucl. Mater. 151 (1988) 269.
[11] K. Nagarajan, Rita Saha, R.B. Yadav, S. Rajagopalan, K.V.G. Kutty, M. Saibaba, P.R. Vasudeva Rao, C.K. Mathews, J. Nucl. Mater. 130 (1985) 242.
[12] X. Yang, Z. Wu, J. Zhao, H. Wang, D. Huang, F. Qin, Vacuum 49 (1998) 139.
[13] E. Papparazzo, Surf. Sci. 234 (1990) L253.

[14] C.D. Wagner, W.M. Riggs, L.E. Davis, J.F. Moulder, G.E. Muilenberg, Handbook of XPS, PE Corporation, USA, 1979.
[15] Santanu Bera, S.K. Sali, S. Sampath, S.V. Narasimhan, V. Venugopal, J. Nucl. Mater. 255 (1998) 26.
[16] M.P. Seah, W.A. Dench, Surf. Interface Anal. 1 (1979) 1.
[17] A.F. Carley, P. Nevitt, P. Roussel, J. Alloys Compd. 448 (2008) 355.
[18] E.S. Ilton, J-F Boily, P.S. Bagus, Surf. Sci. 601 (2007) 908.
[19] A. Pfau, K.D. Schierbaum, Surf. Sci. 321 (1994) 71.
[20] M.L. Trudeau, A. Tschope, J.Y. Ying, Surf. Interface Anal. 23 (1995) 219.
[21] J.P. Holgado, R. Alvarez, G. Munuera, Appl. Surf. Sci. 161 (2000) 301.
[22] M. Romeo, K. Bak, J.El. Fallah, F. Le Normad, L. Hilaire, Surf. Interface Anal. 20 (1993) 508.
[23] H. Norenberg, J.H. Harding, Surf. Sci. 477 (2001) 17.
[24] C. Muggelberg, M.R. Castell, G.A.D. Briggs, D.T. Goddard, Appl. Surf. Sci. 142 (1999) 124.